Consideration of wall roughness effects in the prediction of heat transfer in rocket combustion chambers

Björn Kniesner, Manuel Frey and Oliver Knab
ASTRIUM GmbH Space Transportation, 81663 Munich, Germany
Bjoern.Kniesner@astrium.eads.net, Manuel.Frey@astrium.eads.net, Oliver.Knab@astrium.eads.net

Abstract

Experimental investigations of several rocket combustion chambers locally show an increase in wall surface roughness with ongoing hot firing operation leading to a perceptible integral heat load increase. This is confirmed by calorimetric measurements. In order to determine the influence of different surface wall roughness values on the local wall heat flux and thus the combustion chamber wall temperature ASTRIUM Space Transportation applies the axisymmetric multi-phase in-house Navier-Stokes solver Rocflam-II. Simulations of several combustion chambers considering the occurring temporally as well as spatially variable roughness development show substantially different wall temperature evolutions compared to former simulations without detailed wall roughness consideration.

Nomenclature

Latin Symbols

A_μ	[-]	Dimensionless model parameter
A^+	[-]	Dimensionless model parameter
k_s	[µm]	Equivalent sand grain roughness
Nu	[-]	Nusselt number
O/F	[-]	Mixture ratio
p	[bar]	Pressure
$\dot{Q}$	[MW]	Integral heat load
$\dot{q}$	[MW/m²]	Local heat flux
R_z	[µm]	Ten-point roughness
R_a	[µm]	Average roughness
T	[K]	Temperature
t	[s]	Time

Greek Symbols

μ_t	[Pa s]	Turbulent viscosity
λ_t	[W/(mK)]	Turbulent conductivity
η_{c^*}	[-]	Combustion efficiency
Ψ	[-]	Pressure loss coefficient

Abbreviations

CFD	Computational Fluid Dynamics
CFX	Commercial CFD solver
EDC	Eddy Dissipation Concept
PDF	Probability Density Function
RANS	Reynolds Averaged Navier Stokes
RCFS-II	ASTRIUM in-house engineering tool
Rocflam-II	ASTRIUM in-house CFD solver

1. Introduction

Though the strong influence of wall roughness on wall heat flux is well known, its effect on life prediction in rocket combustion chambers is seldom considered in detail. In literature no contribution concerning this issue could be found. The current status at ASTRIUM is that the experimentally determined heat load increase is globally taken into account for the design process. The fact, however, that this heat load increase is to the biggest part caused by locally limited and thus very strong wall roughness increases is up to now neglected. This also means that the locally occurring wall temperatures become significantly greater than a comparable constant wall roughness increase over the whole combustion chamber length.
The aim of this paper is the quantification of the engine specific wall roughness increase depending on time and space in order to give a realistic prediction of the expected wall temperature by application of a numerical simulation method.

Doing so, it is clear that the surface roughness increase is driven by multiple influencing factors. Besides the chamber wall material the wall temperature itself as well as the load duration play a decisive role. But also the near wall velocity and thus wall shear stress as well as gas composition are important parameters. Due to the fact that a detailed experimental investigation is very costly and complicated in the frame of full-scale rocket engines the current work focusses on already existing experimental information. These are in principal surface roughness measurements, calorimetric local wall heat flux as well as integral heat load measurements within the cooling circuit of the engine.

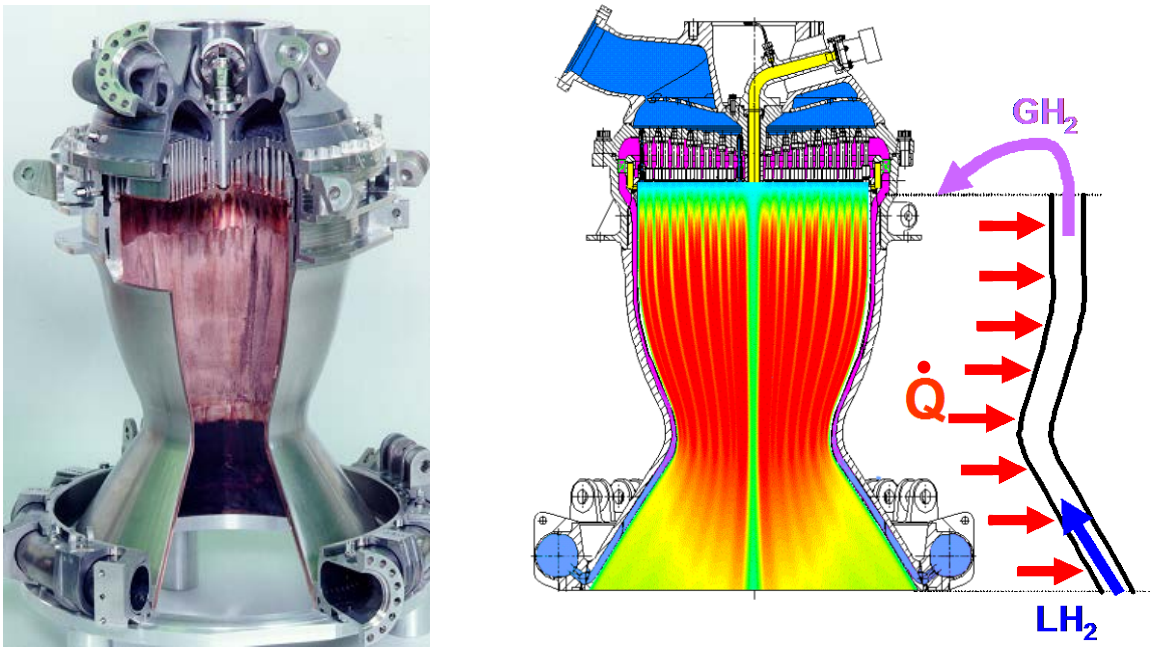

Figure 1: Sliced combustion chamber with well visible wall roughness (left) and sketch showing the coupled heat transfer problem in rocket combustion chambers (right)

2. Modeling Approach

For the prediction of wall temperature ASTRIUM Space Transportation applies on the hotgas side the axisymmetric Euler/Lagrange multiphase Navier-Stokes-Solver Rocflam-II [2]. With Rocflam-II the simulation of flow, evaporation and combustion for nearly arbitrary propellant combinations in axisymmetric rocket combustion chambers is possible. Therefore an equilibrium based Presumed Probability Density Function (PPDF) method or a non equilibrium global chemistry model based on an Eddy Dissipation Concept (EDC) can be applied. Both methods use a low-Re k-ε turbulence model in a 2-layer formulation, applying only the k-equation in the near wall region whereas ε is computed from an algebraic expression [5], [6]. The implemented wall roughness model uses the equivalent sand grain roughness k_s and is supported by the dimensionless parameter A_μ which modifies the damping function for the turbulent viscosity near the wall. A large value of A_μ reduces the turbulent length scale l_μ and thus the turbulent viscosity μ_t (eq. 1). By this the boundary layer characteristic of a smooth wall is approximated. The other way round, by using small values for A_μ a rougher wall is simulated. The zero wall value of the turbulent viscosity as well as the turbulent kinetic energy is conserved. The parameter A^+ can be used to capture pressure gradient effects in the boundary layer. However, in the considered cases the standard value of $A^+=25$ is applied.

$$\text{(eq. 1)} \qquad \mu_t = C_\mu \rho l_\mu \sqrt{k} \quad \text{with} \quad l_\mu = C_l \delta y \left[1 - \exp\left(-\frac{\mathrm{Re}_y}{A_\mu} \frac{25}{A^+} \right) \right]$$

For the determination of the wall temperature evolution additionally to the hot gas side computation the cooling circuit has to be simulated as well. For this purpose, in the presented cases the Nusselt based in-house tool RCFS-II [1] is utilized. Both programs are loosely coupled by exchange of wall temperature and heat flux (conjugate heat transfer).

For visualization of the conjugate heat transfer problem in rocket combustion chambers a rocket engine with injection head and cooling circuit is shown in Figure 1. The hot gas side heat flux $\dot{q}$ heats up the cooling fluid. By this, the wall temperature and in turn the heat flux are influenced. As soon as the coupling is converged, heat flux, wall temperature and coolant temperature rise have adjusted themselves in a consistent manner.

3. Calibration of the roughness model

For the application of the presented wall roughness model it is essential to know which value of A_μ in the damping function (eq. 1) corresponds to which surface roughness value. In literature, several different value of A_μ are given which in addition are not linked to real surface or equivalent sand grain roughness values. For this reason, in a first step, a numerical experiment has been set up in order to establish a correlation between the factor A_μ and values of an equivalent sand grain roughness. In a second step the experimentally measured technical surface roughness has to be transferred into an equivalent sand grain roughness.

3.1 Analytical side

For the correlation between A_μ and the sand grain roughness several numerical simulations of a fully developed pipe flow where carried out. In these computations the sand grain roughness as well as the Reynolds number have been varied. The gas composition and the Reynolds numbers are chosen in a way to be characteristic for the combustion chambers manufactured at ASTRIUM. By comparison of the achieved pressure drop with theoretical values (Colebrook [9] / Moody diagram [10]) a relation between the equivalent sand grain roughness k_s and the model parameter A_μ could be established. The achieved analytical correlation is described by an exponential function [3]:

$$\text{(eq. 2)} \qquad A_\mu = -B \ln\left[\frac{k_s}{16}\right] \quad \text{or} \quad k_s = 16\, e^{-A_\mu / B}$$

As Nunner [8] and later Dipprey and Sabersky [7] showed, the influence of surface roughness on heat transfer is not as strong as its influence on momentum. This means that models such as the one used in Rocflam-II, determining the turbulent conductivity by a gradient diffusion hypothesis and thus by the turbulent viscosity,

$$\text{(eq. 3)} \qquad \lambda_t = \frac{\mu_t c_p}{\mathrm{Pr}_t}$$

over-estimate the influence on heat transfer, when using a constant turbulent Prandtl number (Figure 2). For compensation of this behavior the prescribed wall roughness is artificially reduced for heat transfer. Thereby, the decreased influence of the wall roughness is accounted for. A comparable result would be obtained by increasing the turbulent Prandtl number in a certain way when approaching the wall. For the calibration of the necessary reduction several pipe flow computations at varying surface roughness values have been conducted.

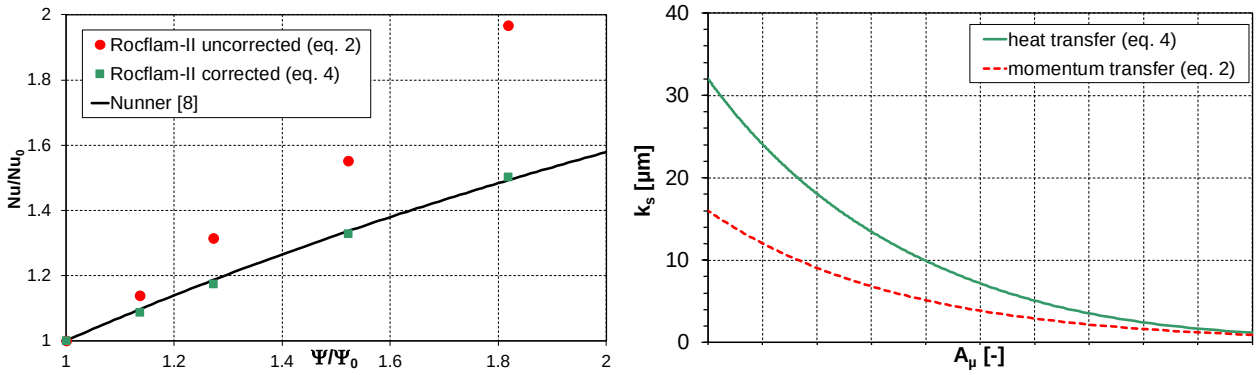

Figure 2: Influence of wall roughness on heat- and momentum transfer according to [8] in comparison to tube flow computations with and without roughness (left) as well as the corresponding correlation between A_μ and k_s (right)

Figure 2 left shows the experimental results of Nunner [8], generated for pipe flows. The ordinate shows the ratio of rough and the smooth pipe Nusselt number. In analogy to this on the abscissa the ratio of friction in the rough and the smooth pipe is displayed. The decreasing slope of Nunner's curve is well represented when applying the correction. The overestimation of the uncorrected curve is well visible, too. Incorporating this correction directly into the roughness correlation $k_s \Leftrightarrow A_\mu$ one obtains a new and different evolution (Figure 2 right):

$$\text{(eq. 4)} \qquad A_\mu = -B \ln\left[\frac{k_s}{16 \cdot (2 - e^{-C k_s})}\right] \qquad \text{with} \qquad k_s = \alpha R_z \approx 6 \alpha R_a$$

Here, α, B and C are constants derived from experimental data. Equation (4) is not explicitely solvable for the equivalent sand grain roughness k_s. The tendency is that the effective value of k_s with respect to heat transfer is half of the value with respect to momentum transfer. This means that in case of heat transfer approximately double the roughness as without correction, i.e. for momentum, can be considered, thus in maximum $k_s \approx 32\mu m$ (Figure 2 right).
Due to the fact that the current work focusses on heat transfer, equation 4 is applied in the following. The influence of wall roughness on pressure drop within the combustion chamber is anyway very low. In a typical chamber an increase of the equivalent sand grain roughness k_s by 100% leads to an increase in pressure drop by about 1.5 per cent only.

3.2 Experimental side

Having established a correlation between A_μ and k_s, the link between the real technical roughness (R_a, R_z) and the equivalent sand grain roughness (k_s) is still missing. The biggest part of the transformation rules that can be found in literature, i.e. Dirling [4], are based on model roughnesses. A direct correlation between real measured surface roughness and equivalent sand grain roughness could not be found. This is actually not surprising because the relation between these two depends on several hardly quantifiable values. In most cases, the sand grain roughness is therefore determined experimentally, for example by comparison of pressure drop in pipe flows with theoretical values. In the present case theses data are not available. Nevertheless, based on the correlations for the model roughness as well as Astrium data on surface roughness and corresponding pressure drop in cooling channels it could be derived, that the equivalent sand grain roughness is equal to a factor times the ten-point roughness value R_z ($k_s = \alpha R_z$). In case only the average roughness value R_a is available, R_z can be obtained by simply using $R_z \approx 6R_a$. This relation could be gathered by comparison of numerous available roughness measurements of both quantities. With this, the correlation of $R_a \Leftrightarrow A_\mu$ is closed.

4. Spatial and temporal roughness evolution

As already mentioned in the introduction the surface roughness develops strongly different over the length of the combustion chamber. Driving parameter is the level of wall temperature of the non-aged chamber at manufacturing roughness as it becomes visible from Figure 3. There, the simulated wall temperature of the non-aged chamber is plotted together with the measured surface roughness profile of the strongly aged chamber for three different rocket engines. For all of the three engines the same copper alloy material is used for the combustion chamber wall.

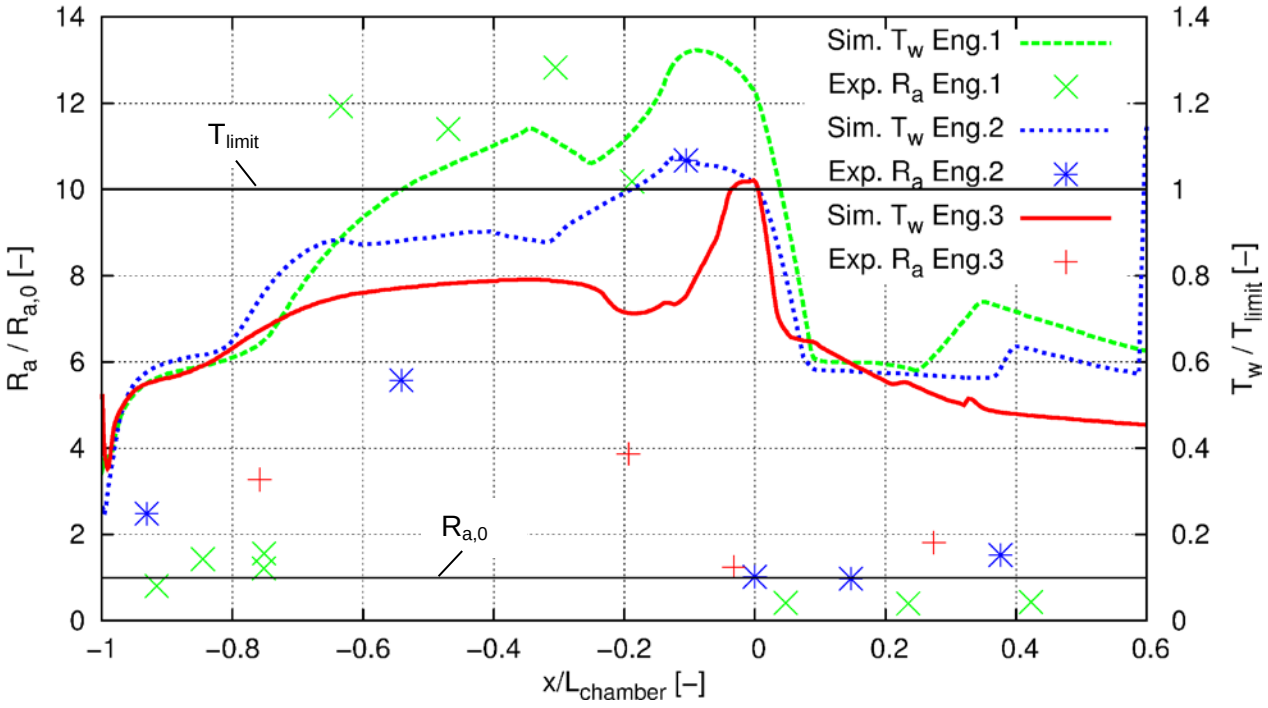

Figure 3: Influence of wall temperature onto the roughness development

Due to the extreme conditions within the combustion chamber measured wall temperatures are not available. Both surface roughness and wall temperature values on the ordinate as well as the axial coordinate on the abscissa are

displayed in non-dimensional form in order to be better comparable. As reference values, an averaged manufacturing roughness $R_{a,0}$ of the combustion chambers as well as a limiting temperature T_{limit} are used. The limiting temperature indicates from which level on the roughness development is strongly supported. Both reference values are indicated by horizontal lines in Figure 3. The axial coordinate is related to the length of the chamber from injector ($x/L_{chamberr}$ =-1) up to the throat which is located at $x/L_{chamber}$=0. In general, one can identify 5 characteristic regions. Depending on the engine, however, not every region is always clearly visible. In the upper left part of Figure 4 one can see where the 5 regions are located within the combustion chamber. In contrast to Figure 3 where the end of operation roughness state is presented, Figure 4 shows the roughness increase as a function of time for a typical engine.
In the divergent part of the chamber – position 5 downstream of the throat – the wall roughness nearly remains at the manufacturing roughness of the new chamber. This holds true even for a long operation time. Nevertheless, locally limited rough spots may occur, but in principle this region stays quite smooth for all the considered engines. Even when moving upstream directly up to the throat no significant roughness development can be observed for any of the engines. This is somewhat surprising because the throat is widely known to be the thermally most critical region of the combustion chamber. However, Figure 3 shows that on the one hand the maximum temperature occurs slightly upstream of the throat, then drastically decreasing downstream due to expansion. On the other hand the strong acceleration and thus high velocity in this region leads to a strong shear stress. By this wall material is disrupted prohibiting a strong roughness evolution.
The region clearly showing the strongest roughness evolution (position 4) starts upstream of the throat near the beginning of the convergent combustion chamber part and ends just upstream of the throat. There, the roughness measurement shows a strong variation. Nevertheless the generally high level is well visible in Figure 4. The positions 2 and 3 which are both located upstream of position 4 in the cylindrical part of the chamber exhibit only a moderate roughness increase. Depending on the geometry of the chamber the length of these two regions varies significantly. For some engines a certain roughness increase can be observed near the injection head (Position 1 in Figure 4).

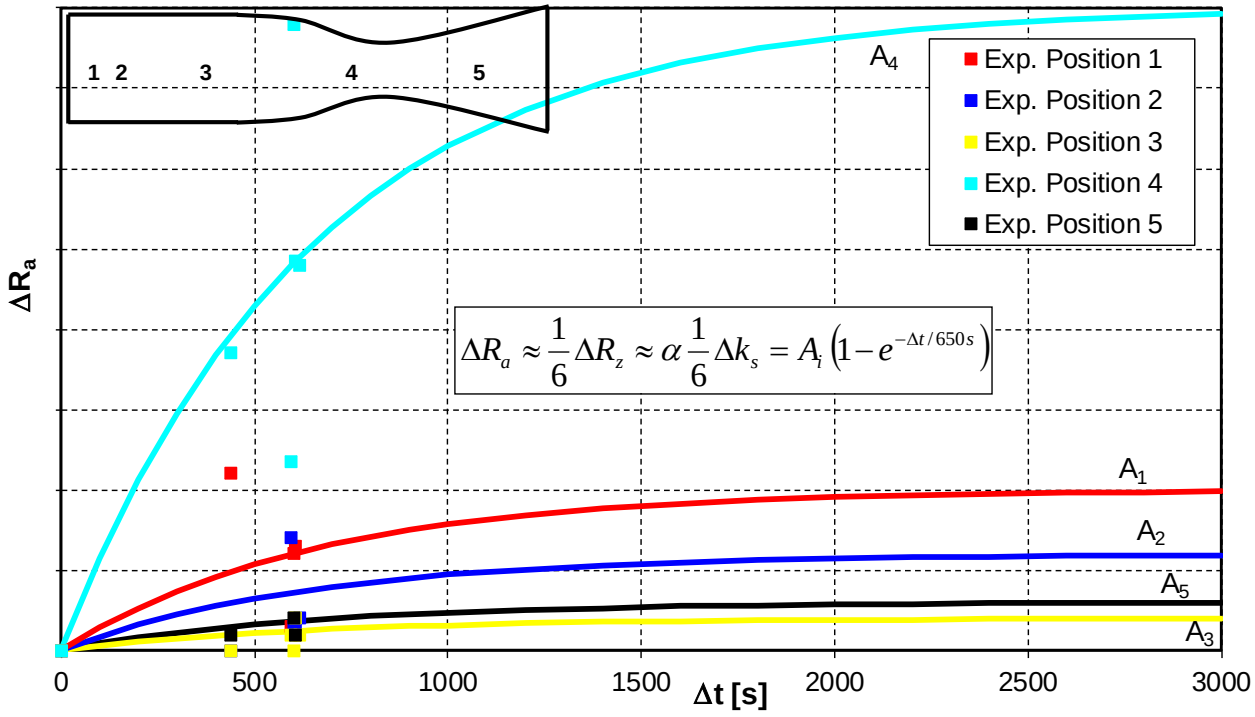

Figure 4: Obtained function for the temporal roughness development at 5 different locations inside the combustion chamber together with measured roughness increase for a typical engine

A crucial role for the correct prediction of the wall heat load is taken by the temporal evolution of the surface roughness. Regarding this it is observed that the roughness starts at the manufacturing roughness and then steadily increases until after certain time saturation is reached. The manufacturing roughness depends on the manufacturing method and the subsequent treatment. For the considered copper alloy chambers it amounts $R_a=R_{a,0}$ roughly. The occurring saturation is due to the fact that from a certain roughness height on, wall material is eroded leading to a roughness decrease which is then increasing again and so on. The fact that wall material is eroded could be confirmed by visual inspection of cutting-samples.
For the analytical description of the temporal roughness evolution an exponential function which reaches saturation after a certain operating time is suitable (see equation in Figure 4). Here, the pre-factor A depends on the axial posi-

tion in the chamber. The starting point for a function of roughness increase with operating time is located at zero for both axes. For fitting of the curve different information is available from measurement. First, the increase in integral heat load within the cooling circuit over operating duration has to be captured. Furthermore, the local heat flux increase which could be extracted from several subscale tests gives valuable information on the temporal and spatial roughness increase. Finally, direct roughness measurements are available. Their informational value, however, is limited. A first reason for this is that nearly all the gathered data is available after about 600s or 10 minutes testing time (Figure 4), as this is the usual operation duration of the considered engines. A second reason is that the measured roughness shows strong scattering. This scattering is caused on the one hand by the fact that it is not possible to measure at exactly the same position before and after each test. On the other hand the chambers partly have strong curvatures, especially in the throat region, so that the roughness measurement is difficult or partly impossible. Nevertheless, in Figure 4 all the data and the finally applied exponential function for a selected engine are shown. Therein, the significant surface roughness development in the regions 1 and 4 corresponding to the already mentioned principal zones of roughness increase is reflected. The formula given in Figure 4 shows the applied exponential function. It depends on the running time Δt and on the considered axial location which is reflected by the use of different A_i values depending on the position (1-5).
For further use of this information in the simulation, a spatial k_s- and corresponding A_μ distribution is generated based on a given manufacturing roughness and a desired operating time of the engine. In order to avoid numerical problems and unphysical heat flux peaks the surface roughness distribution should be as smooth as possible. Therefore, a smooth transition is realised between two locations for which the temporal evolution is known (Figure 5). Generally, the form of the exponential function is dependant on a specific engine.

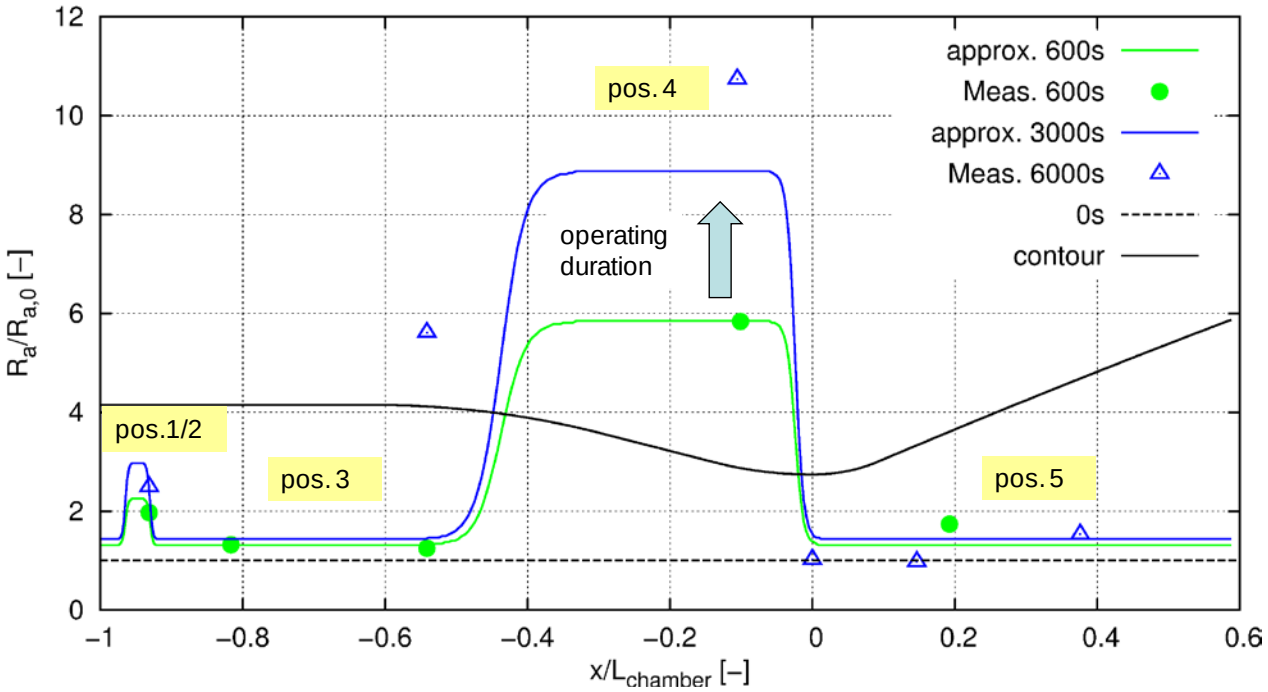

Figure 5: Exemplary approximated evolution of the applied wall roughness for two different operating durations

5. Roughness prediction on basis of wall temperature evolution

Important for the design of new combustion chambers is the possibility of predicting the expected temporal surface roughness evolution in advance on the basis of numerical simulations. Doing so, a more detailed analysis of the chamber life and performance expectation can be carried out in an early design stage. Figure 3 demonstrates that wall temperature is one of the main influencing factors for the wall roughness increase on the hot gas side. As already mentioned in the introduction also the wall material itself as well as the gas composition near the wall play an important role. All the considered roughness measurements originate from copper alloy chambers so that the prediction model is restricted to this material. Furthermore, as the influence of the gas composition, i.e. oxidation or reduction of the surface, on the roughness development has not yet been sufficiently investigated, its influence is not captured by the current prediction model. The implicitly underlying gas composition thus corresponds to a slightly fuel-rich H_2/O_2 combustion (O/F≈6-8) of the experiments. Finally, the established prediction model is only related to the local hotgas wall temperature. The basis of this model is illustrated in Figure 6. It shows the measured maximum wall

roughness increase in dependence on the simulated wall temperature assuming a non-aged chamber at manufacturing roughness. The data originates from a synthesis of the available roughness measurements of Astrium's rocket combustion chamber portfolio.

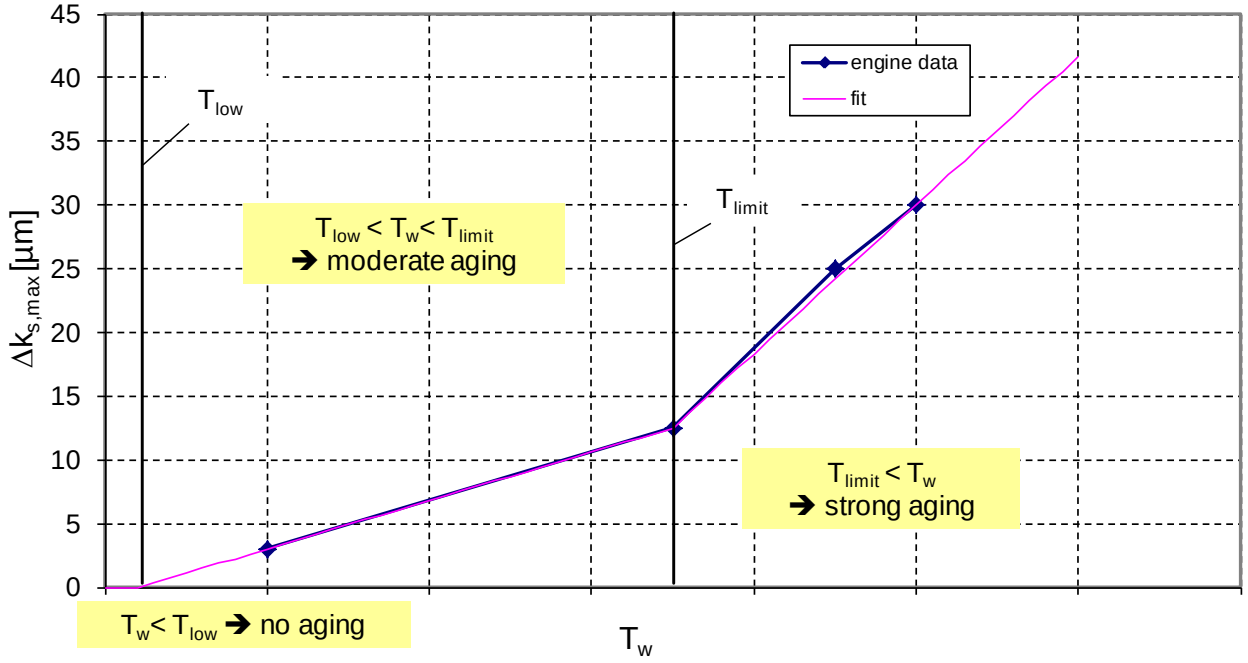

Figure 6: Measured maximum wall roughness increase in dependence on the simulated wall temperature of the non-aged chamber at manufacturing roughness

The diagram is split into three regions. For wall temperatures above T_{limit} the surface roughness increase over operating duration and thus aging is very strong. Below this temperature in the middle region a moderate increase can be expected. Both regions are modelled by a linear dependency with different slopes. This leads to an intersection point with the abscissa at a certain lower temperature limit. Below this limit independently on the hot firing duration of the engine no roughness development occurs in the model. Figure 7 demonstrates the difference between the approximated wall roughness evolution based on available measurement data on the one side and the result of the roughness prediction model (Rocflam-II) only based on the computed smooth wall temperature on the other side. The dashed black line which is identical for both methods corresponds to the initial manufacturing roughness. For a hot firing duration of 600s (green) and 3000s (blue) three main differences can be observed:

- In the front region near the faceplate the measurement shows a moderate but well visible roughness development. This position corresponds to position "1" in Figure 4. The wall temperature in this area stays low due to the propellant preparation leading to a small or even not existent surface roughness increase in the case of the prediction model. Consequently an additional, not considered parameter has to play a role. Most probably it is a matter of an interaction between the injector and the wall which can up to now not be fully described.

- The evolution of the roughness in the cylindrical and convergent section of the chamber is a problem in general as the few available roughness measurements do not allow a clear picture of the detailed axial roughness profile. In addition, even at a fixed axial location different roughness values occur over the circumference due to three-dimensional effects. The approximated evolution finally was chosen in a way that the steep roughness increase is linked to an optically well visible discoloration line within the chamber. In the prediction model the roughness profile follows the wall temperature which increases flatter but further upstream. However, in the throat region which is the critical for the chamber life duration the maximum values of both are comparable.

- In and directly downstream of the throat the measured roughness is generally low. This is linked to the high shear stress and strongly decreasing pressure and temperature in this region. In the prediction model the strong decrease of the roughness is slightly delayed resulting in a relatively elevated roughness even in the throat.

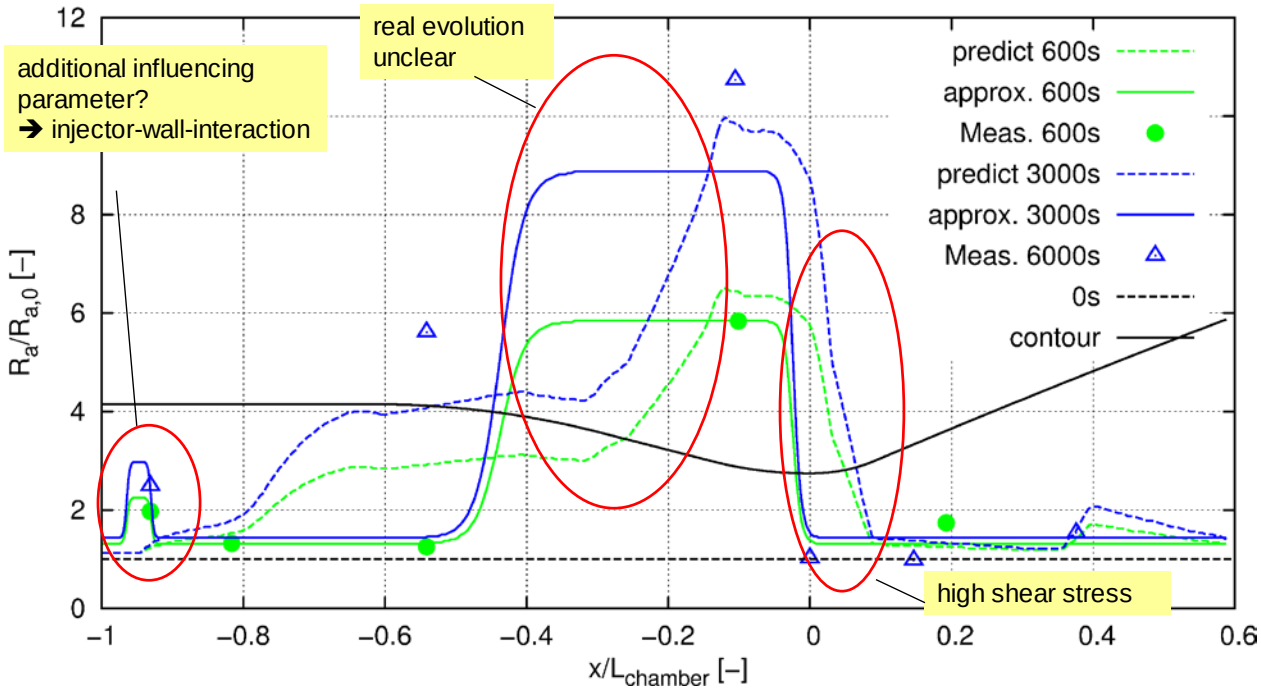

Figure 7: Difference between the approximated roughness evolution on basis of roughness measurements (solid lines) and predicted evolution based on the initial wall temperature (dashed lines)

6. Application of wall roughness evolution model

In the following the results of different combustion chamber simulations using the above introduced roughness functions are shown and discussed for three different rocket engines. In all cases the initial state at manufacturing roughness (0s) is compared to a moderate (nominal operational – 600s) and a final, maximal reachable surface roughness state. For each engine an individual but constant load point is used for all three operating durations. In order to get an impression of the realized axisymmetric multiphase CFD simulations Figure 8 shows a contour plot of temperature and mixture fraction for an example thrust chamber.

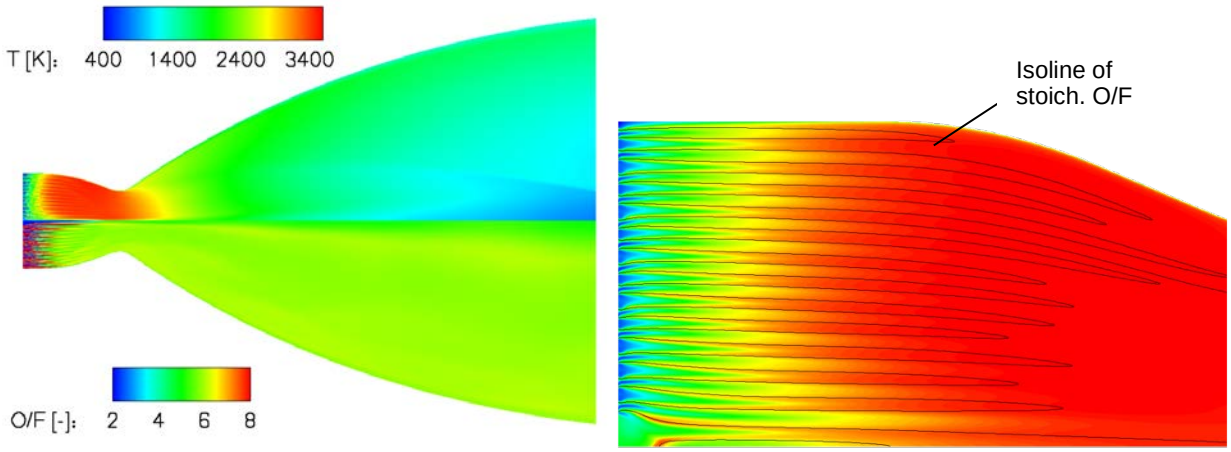

Figure 8: Contour plot of temperature and mixture ratio (left) as well as zoom on the combustion chamber region together with isolines of stoichiometric mixture ratio (right)

By means of the high temperatures (red) one can well notice the region of combustion. In this zone the wall temperature as well as the wall heat flux are on an elevated level as could already be seen in Figure 3. Additionally, the strong temperature decrease in the divergent part due to expansion is visible by means of the temperature scale. The mixture ratio between oxidizer and fuel on the left side of Figure 8 shows that the propellant preparation and subse-

quent mixing in the chamber up to the throat is quite well. The injection region is additionally enlarged on the right side of Figure 8. One can clearly see the single injection rows distributed over the chamber radius. Directly at the faceplate the temperature stays moderate. With increased mixing the situation quickly changes. The best mixing is achieved in the shear layer between oxidizer and fuel. Mainly here combustion takes place as is visualized by the isoline of stoichiometric mixing ratio.

6.1 Engine 1

As already visible in Figure 3, engine 1 shows the strongest surface roughness increase. This is mainly due to the elevated wall temperature as likewise visible in Figure 3. Additionally, for this engine so-called "blanching" was observed. This means that caused by the relatively short cylindrical part of the combustion chamber oxidizer from the outer element row impacts on the wall in the convergent part of the chamber leading to increased thermochemical effects. Figure 9 shows the wall temperature for three simulations at the already introduced initial, moderate and final roughness states. The differences above all at the end of the cylindrical section and the convergent part of the chamber are huge. The wall temperature increases about 30% thus amplifying the roughness development. At a certain stage (≈5000s in the present case) surface erosion begins and the roughness development saturates.

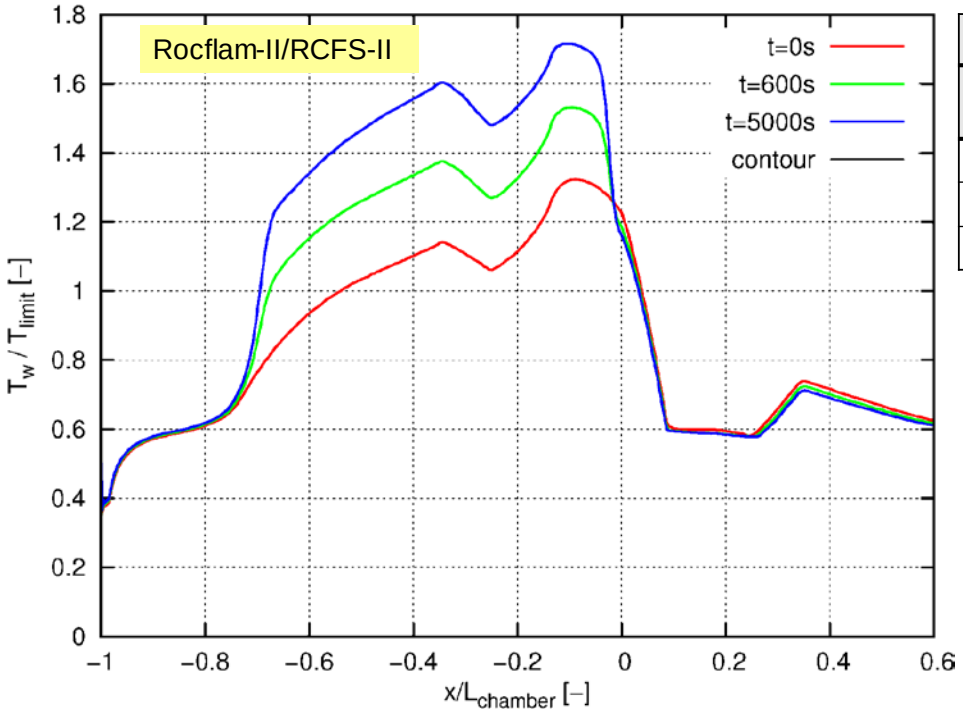

simulation results	
A_μ [-]	$\Delta\dot{Q}$ [%]
f(x,0s)	0
f(x,600s)	12
f(x,5000s)	24

$$\Delta\dot{Q}_{exp,5000s} \approx 20-25\%$$

Figure 9: Computed (Rocflam-II/RCFS-II) hot gas wall temperature of engine 1 after different operating durations

The increasing material erosion together with additional degradation mechanisms, i.e. dog-house effect, leads to cracks in the hotgas wall after a certain operational time and a certain number of hot firing runs. As a consequence to the crack the cooling fluid – in the present case cryogenic hydrogen – leaks from the coolant system into the chamber, building a kind of film cooling and protecting the wall. Thus the combustion chamber wall temperature decreases, preventing the failure of the chamber by this self-healing process. Nevertheless, in flight the chamber is operated in its 2nd to 4th cycle for which it is ensured that no cracks occur. In contrast to the convergent part nearly no temperature rise can be recognized directly in the throat which is due to the fact that the roughness development stays small there as has already been discussed in the previous section. The table on the right of Figure 9 also shows the experimentally measured relative change in integral heat load of the chamber with increasing run time. The simulation using the wall roughness evolution model shows an integral heat load increase $\Delta\dot{Q}$ of 24% after an operating duration of 5000s, which agrees well to the measured values of 20-25%.

6.2 Engine 2

The wall temperature level of the second considered engine lies below the one of the first engine (Figure 10).

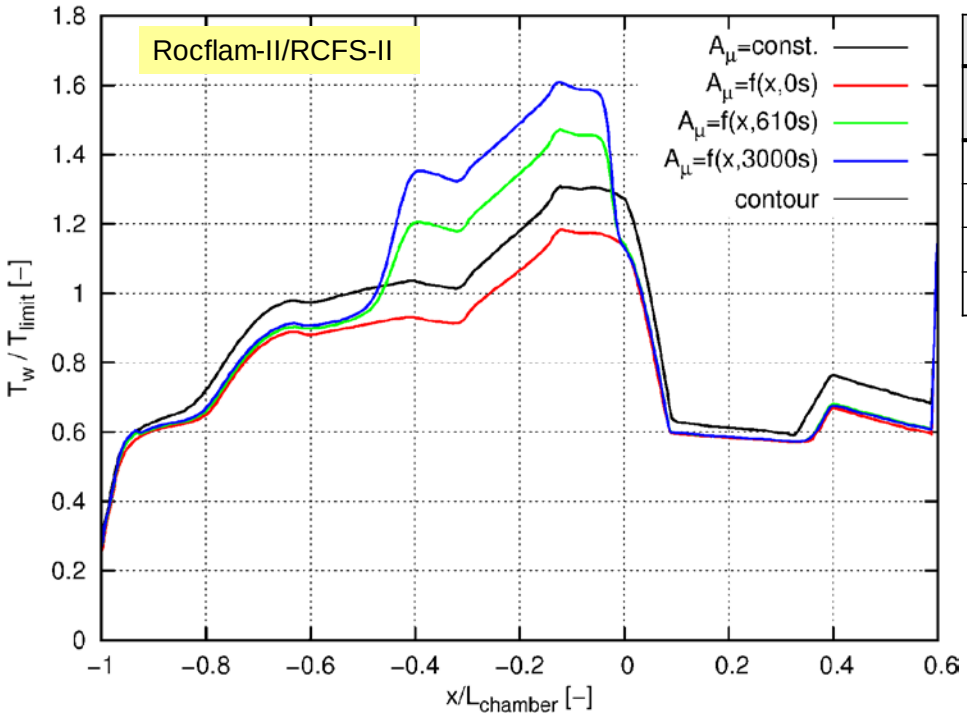

simulation results	
A_μ [-]	$\Delta\dot{Q}$ [%]
const.	10
f(x,0s)	0
f(x,610s)	12
f(x,3000s)	18

$$\Delta\dot{Q}_{exp,3000s} \approx 12-15\%$$

Figure 10: Computed (Rocflam-II/RCFS-II) hot gas wall temperature of engine 2 after different operating durations

In addition, the saturation of the roughness development is reached after 3000s already compared to 5000s in the previous case. As a consequence, the temperature increase at 600s in no longer situated in the middle between initial and final roughness but already close to the final one. Except for the injection region the wall temperature evolutions for both engines are very similar. However, close to the face plate an additional roughness increase is visible for the second engine. Nevertheless its contribution is small and mainly visible not until the final roughness is reached after 3000s. Corresponding to the lower wall temperature level for the initial case also the wall roughness increase and thus the increase in integral heat load stays below the one of engine 1. At 610s an increase of 12% is computed. The absolute value of the integral heat at this aging state slightly overpredicts the experimental value at 610s. In maximum about 18% increase are predicted. Again, in experiment a lower value of only up to about 15% is measured. A possible reason for this is a not completely correct axial roughness distribution which is anyway hard to reconstruct on the basis of the relatively few available roughness measurement. Given this uncertainty the agreement is nevertheless good.
In order to get an impression of the former modelling with constant, moderate roughness the black line is also included in Figure 10. Integrally seen, this computation is comparable to the green one of 610s. However, one can clearly recognize the effect of local roughness modelling on wall temperature. The difference adds up to well above 100K in the region of the maximum temperature, for the final roughness value even to roughly 200K. This in turn depicts a completely new situation for the material load and life evaluation of this chamber.
All simulations presented up to now used the 1D engineering tool RCFS on the coolant side. Switching now to a Rocflam-II/CFX coupling which resolves the cooling circuit threedimensionally in detail, the maximum temperature level even further increases. This is illustrated in Figure 11 for the initial and the final surface roughness. The main reason for the higher wall temperature in the detailed computation is the consideration of inflow-, curvature- and stratification- effects. Driven by the higher wall temperature the absolute value of the wall heat flux slightly decreases. Nevertheless, the relative increase from initial to final roughness slightly rises to 19%. This means that also for this engine the integral heat load increase is slightly overpredicted and thus conservative with respect to the life estimation based on the maximal hotgas wall temperature.

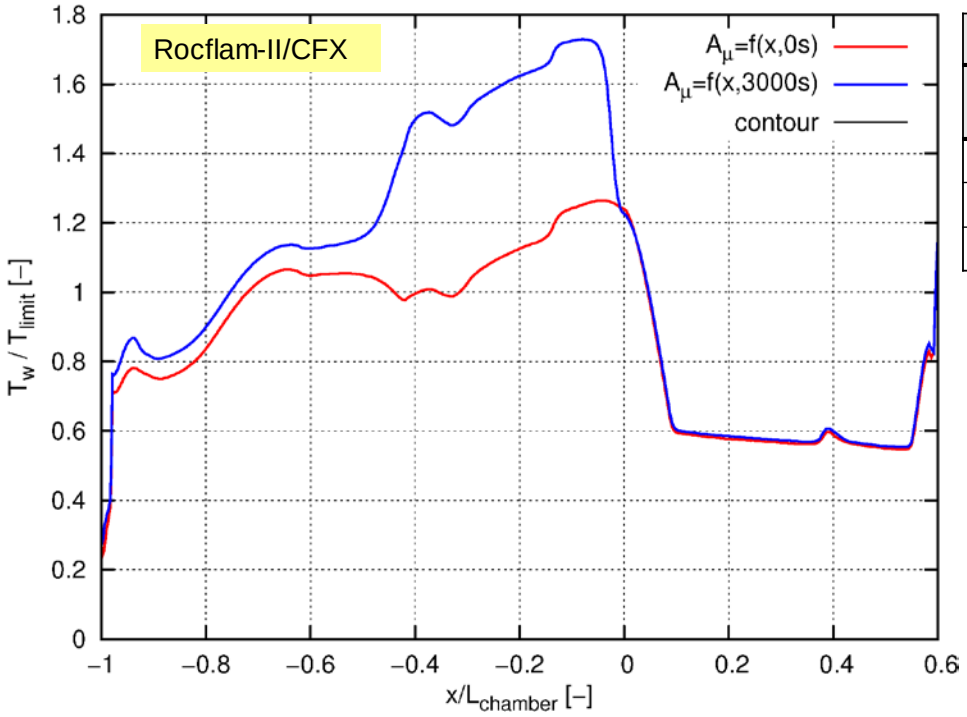

simulation results	
A_μ [-]	$\Delta\dot{Q}$ [%]
f(x,0s)	0
f(x,610s)	-
f(x,3000s)	19

$$\Delta\dot{Q}_{exp,3000s} \approx 12-15\%$$

Figure 11: Computed (Rocflam-II/CFX) hot gas wall temperature of engine 2 after different operating durations

The effect of using the wall temperature based prediction model for the roughness development is visible in Figure 12. Using the example of the already shown Rocflam-II/RCFS-II coupling (Figure 10) one can see the impact of the two different roughness distributions from Figure 7 on the wall temperatures which show an analogous behaviour. Corresponding to the slightly higher maximum roughness in case of the prediction model the maximum value of the wall temperature is as expected also higher.

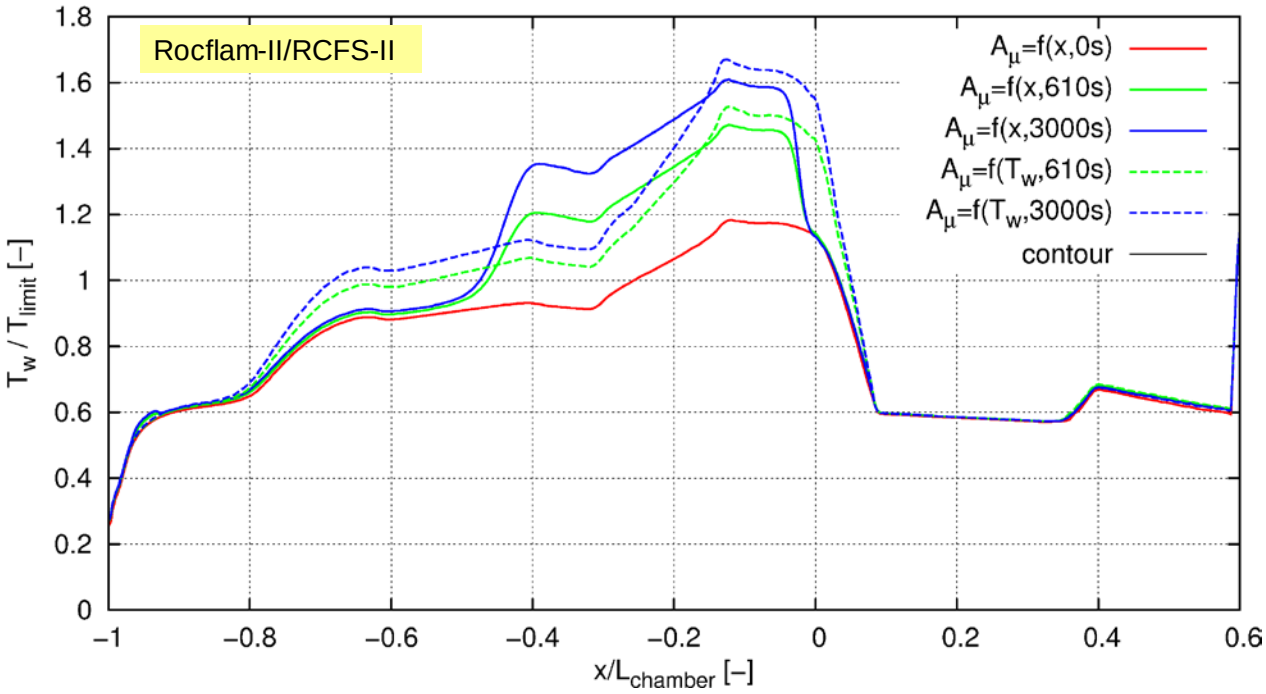

Figure 12: Differences in hot gas wall temperature of engine 2 at different operation durations using the approximated wall roughness evolution (solid lines) on the one and the prediction model (dashed lines) on the other side

6.3 Engine 3

Due to special design characteristics the wall temperature level of the third and last example engine is substantially lower than in the two previous cases. A significant wall roughness increase only occurs after high load points. Running lower load points afterwards, the surface roughness does not further increase. For this reason, Figure 13 does not show the classical roughness development but a specific load point before and after a high load point in between. By looking at the increase in wall temperature one can notice that the roughness develops similarly to both of the already presented examples, mainly from the middle of the chamber up to the throat, most in the convergent part. Additionally, there is a rough region upstream not as close to the faceplate as for the first two engines. The measured roughness in this area is higher as in the previous cases which is reflected in the wall temperature in this region. As mentioned before the wall roughness does not further increase when running the considered load point.
The predicted rise of integral heat load due to the measured surface roughness increase adds up to approximately 8% (Figure 13). In experiment a difference of 6%-7% was measured. The absolute values of integral heat load also match very well for simulation and experiment in this case.

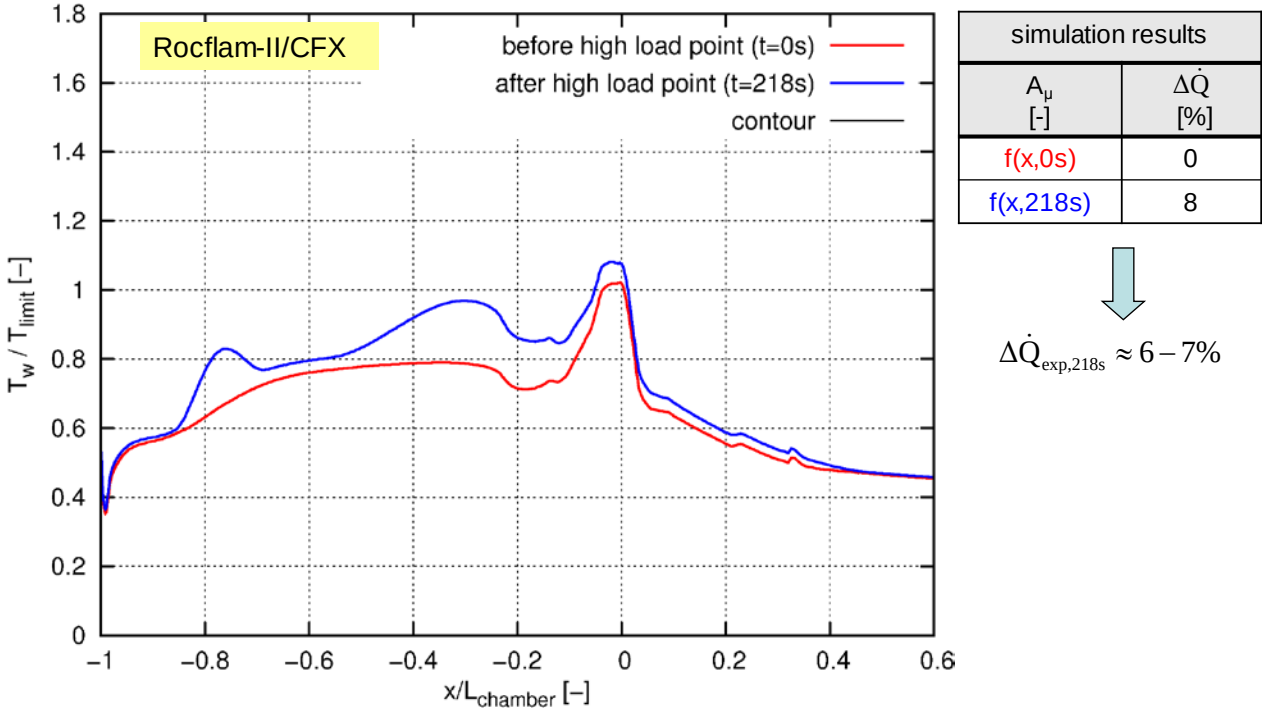

Figure 13: Computed (Rocflam-II/CFX) hot gas wall temperature of engine 3 before and after a high load point in-between

7. Summary and conclusions

Rocket combustion chamber testing has exhibited that thermally highly loaded walls degrade over hot firing time. Thus, wall heat flux and wall temperature computations have to take into account a temporally evolving wall roughness. As consequence, predictive tools for heat transfer and liner life must have the capability to handle wall roughness influence and need a model which describes how the wall roughness develops locally over time. Otherwise, temporal heat load increase as well as liner life-time cannot be predicted accurately.
Within the framework of the presented work available experimental data has been used to establish a combustion chamber liner roughness model considering the location as well as operating duration for numerical simulations of rocket combustion chambers. The application of this model to three different rocket engines having a copper-alloy liner demonstrates that the difference in integral heat load to the combustion chamber wall due to wall roughness increase can reach values of up to 25%. Therefore, it is essential to consider this degradation effect for the simulation of tests, predesign of new chambers, specification of heat loads and life analysis. The situation becomes even more severe looking at the resulting local wall temperature development. It turns out that the biggest part of the roughness increase is limited to a region approximately from half of the combustion chamber cylinder down to the throat. This in turn means that the local wall heat flux and thus wall temperature increase has to be much stronger than the integral one.

In order to improve the predictability of the wall heat flux, wall temperature and thus life expectation of the chamber a simple prediction model has been established based on the available test data. With this model it is possible to conclude locally on the maximally expected surface roughness as well as arbitrary time-dependent states in-between only on the basis of the computed wall temperature for the new chamber at initial wall roughness. In this context, the exclusive usage of the wall temperature solely implies the limitation of applicability to copper-alloy chambers operated by H_2/O_2 at mixture ratios of 4 to 8.

8. Acknowledgment

The Authors like to thank the Bavarian Research Foundation (BFS) for financing of the project "Lebensdauer thermomechanisch belasteter Bauteile" within which most of the results have been gained.

9. References

[1] Mäding, C., Wiedmann, D., Quering, K. and Knab, O.: "Improved Heat Transfer Prediction Engineering Capabilities for Rocket thrust Chamber Layout", EUCASS2009-90, 3rd European Conference for Aerospace Sciences (EUCASS), Versailles, France, 2009

[2] M. Frey, T. Aichner, B. Ivancic, B. Kniesner and O. Knab, "Modeling of Rocket Combustion Devices," in 10th AIAA/ASME Joint Thermophysics and Heat Transfer Conference, Chicago, Illinois, USA, 2010Aupoix, B., Spalart, P. R. "Extension of the Spalart-Allmaras turbulence model to account for wall roughness", Int. J. Heat and Fluid Flow, Vol. 24, Number 4, pp. 454-462, 2003

[3] B. Kniesner, M. Frey., O. Knab, Vorhersage des Wandtemperaturverlaufes in Raketenbrennkammern unter Berücksichtigung zeitlicher und örtlicher Wandrauhigkeits-entwicklungen, Deutscher Luft- und Raumfahrt Kongress 2010, Hamburg, Germany, 2010

[4] Dirling, R. B. "A Method for computing rough wall heat transfer rates on reentry nosetips", AIAA 8th. Thermophysics Conference, pp. 73–763, 1973

[5] Patel, V. C., Rodi, W., Scheurer, G., "Turbulence models for near-wall and low Reynolds number flows - A review", AIAA Journal 23, pp. 1308–1319, 1984

[6] Wolfshtein, M.W. "The velocity and temperature distribution in one-dimensional flow with turbulence augmentation and pressure gradient", Int. J. Heat and Mass Transfer, Vol. 12, pp. 301-318

[7] Dipprey, D. F.; Sabersky, R. H. "Heat transfer and friction in smooth and rough tubes at various Prandtl numbers", Int. J. Heat Mass Transfer, Vol.6, pp. 329-353,1963

[8] Nunner, W. "Wärmeübertragung und Druckabfall in rauhen Rohren", VDI-Forschungsheft 455, 1956

[9] Colebrook, C.F. "Turbulent flow in pipes, with particular reference to the transition region between smooth and rough pipe laws". Journal of the Institution of Civil Engineers (London), 1939

[10] Moody, L.F. "Friction Factors for Pipe Flow". Transactions of the ASME 66 (8): 671–684, 1944